small NANO MICRO

Graphene Oxide

Mechanism Studies on the Superior Optical Limiting Observed in Graphene Oxide Covalently Functionalized with Upconversion $NaYF_4$:Yb^{3+}/Er^{3+} Nanoparticles

Tingchao He, Wei Wei, Lin Ma, Rui Chen, Shixin Wu, Hua Zhang, Yanhui Yang, Jan Ma, Ling Huang, Gagik G. Gurzadyan,* and Handong Sun**

The increased utilization of high power laser sources has rendered great challenges for designing efficient optical limiting (OL) materials to protect human eyes and various delicate optical devices. An ideal optical limiter should greatly attenuate an intense laser beam while exhibiting high transmittance for low-input optical intensity.[1] Up to now, numerous organic and inorganic materials have proved to be good candidates for optical limiters with different working mechanisms. Among them, carbon-based materials, such as fullerenes, carbon black, and carbon nanotubes, have exhibited very good OL performance.[2–5] As a typical representative, graphene, which consists of sp^2-hybridized carbon atoms with single-atom thickness and 2D structure, has exhibited unique electronic, optical, and mechanical properties.[6] The interband optical transitions in graphene are independent of frequency over a wide range and depend only on the fine-structure constant, thus it is naturally promising as a broadband optical limiter.[7] Another important advantage of graphene-based materials is that they can be easily functionalized with organic molecules and hybridized with inorganic nanomaterials via covalent bonding, to improve their OL performances through the synergistic effect. For example, the enhanced nonlinear optical properties have been reported in porphyrin-functionalized graphene,[8] organic dye ionic complex,[9] oligothiophene,[10] fullerene,[11] phthalocyanine,[12] and CdS quantum dots.[13]

Dr. T. He, L. Ma, Dr. R. Chen, Prof. G. G. Gurzadyan, Prof. H. Sun
Division of Physics and Applied Physics
School of Physical and Mathematical Sciences
Nanyang Technological University
Singapore 637371, Singapore
E-mail: gurzadyan@ntu.edu.sg; hdsun@ntu.edu.sg
W. Wei, Prof. Y. Yang, Prof. L. Huang
School of Chemical and Biomedical Engineering
Nanyang Technological University
Singapore 637457, Singapore
E-mail: lhuang@ntu.edu.sg
Dr. S. Wu, Prof. H. Zhang, Prof. J. Ma
School of Materials Science and Engineering
Singapore 639798

DOI: 10.1002/smll.201200249

We have noticed that all the OL properties of graphene-containing materials, usually dispersed in liquid media, have been studied only under nanosecond excitation conditions and the working wavelengths of the lasers used are mainly 532 or 1064 nm.[7–13] However, the studies on the OL properties of graphene-containing materials in femtosecond region and other wavelengths are still absent. To a large extent, it may be due to the saturable absorption behavior of graphene under the excitation of femtosecond laser with low frequency.[14,15] Though most of the materials reported have shown good OL behavior in the nanosecond region due to the dominance of nonlinear scattering (NLS), they suffer from the dramatic decrease of OL performance due to the strongly suppressed NLS effect when fabricated into solid films or excited with femtosecond pulse, which remains a serious obstacle for real applications. Therefore, design and synthesis of novel graphene-based OL materials that can work in the femtosecond pulse domain and other wavelengths region still represents a significant challenge.

Due to the long lifetime (in the order of milliseconds) of their real metastable states, upconversion process of lanthanide (Er^{3+}, Yb^{3+}, and Tm^{3+}) ions doped in the lattice of $NaYF_4$ nanocrystals after near infra-red (NIR) laser excitation, can be nearly 10^5 times more efficient than the typical two-photon absorption process observed in organic molecules.[16] Therefore, it is highly possible to synergize the NLS effect of graphene oxide (GO) with the unique upconversion effect of rare earth nanoparticles and develop a novel nanocomposite working at a broadened channel for OL where the NIR excitation energy can be efficiently absorbed by $NaYF_4$:Yb^{3+}/Er^{3+} nanocrystals. Herein, we report the mechanisms of the superior OL effect observed from the GO covalently functionalized with $NaYF_4$:Yb^{3+}/Er^{3+} nanoparticles (abbreviated as GO-Er) under 800 nm femtosecond pulses (100 fs, 80 MHz) excitation.

Figure 1a shows the UV-Vis absorption spectra of $NaYF_4$:Yb^{3+}/Er^{3+} nanoparticles synthesized without GO (abbreviated as $NaYF_4$:Yb^{3+}/Er^{3+}), pure GO and GO-Er dispersed in ethanol/water solution (1/1, v/v). The absorption peak at 229 nm is assigned to π–π* transition of the C=C bonds in GO sample and the shoulder at 300 nm is due to the n-π* transition.[17] In GO-Er solution, the absorption peak of GO shifts from 229 nm to 276 nm, suggesting the apprearance

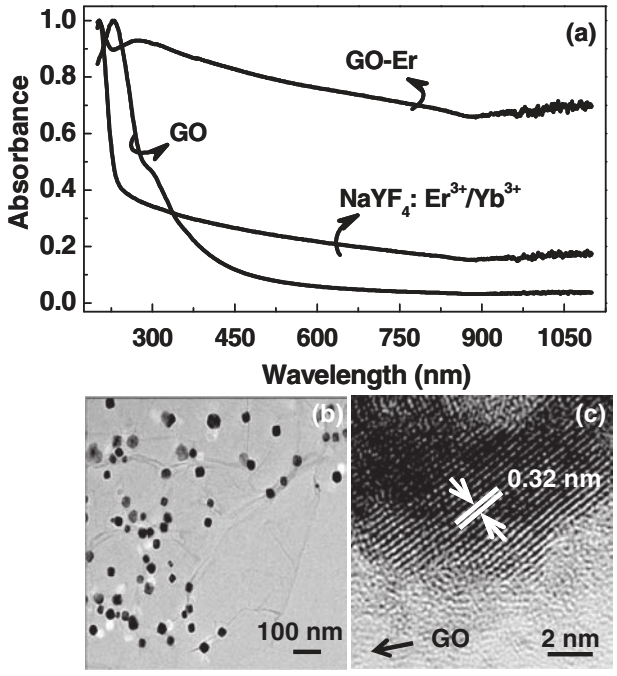

Figure 1. a) UV-Vis absorption spectra of GO, $NaYF_4$:Yb^{3+}/Er^{3+} nanoparticles, and GO-Er in ethanol/water solution (1/1, v/v). b) Transmission electron microscopy (TEM) image of GO-Er nanocomposite, and c) high resolution TEM (HRTEM) image of $NaYF_4$:Yb^{3+}/Er^{3+} nanoparticles distributed on GO surface.

of reduced graphene oxide (rGO) which happened during the synthesis process.[18] In addition, compared to GO and $NaYF_4$:Yb^{3+}/Er^{3+} nanoparticles, the absorption band of GO-Er becomes much broader in the whole spectral region, indicating the greatly extended π-conjugation of the nanocomposite in the presence of $NaYF_4$:Yb^{3+}/Er^{3+} nanoparticles.[19] From the TEM images of GO-Er (Figure 1b), it is obvious to see that $NaYF_4$:Yb^{3+}/Er^{3+} nanoparticles distributed uniformly on GO surface, proving the formation of the uniform GO-Er nanocomposite. In the HRTEM image (Figure 1c), the ordered-lattice fringe of 0.32 nm corresponding to the (111) lattice plane of $NaYF_4$:Yb^{3+}/Er^{3+} nanocrystals suggesting that the nanocrystals on GO are in α-phase.

The measurement of the OL performances of all the materials were carried out in a home-built optical system as shown in **Scheme 1**. Using this setup, we can simultaneously investigate the details of both nonlinear transmittance and NLS. Moreover, the nonlinear refraction and two-photon absorption can also be determined by changing the position of samples near focus point (Z-scan measurements).[20] The detailed description of the measurments can be found in experimental part.

Figure 2a shows the OL curves of $NaYF_4$:Yb^{3+}/Er^{3+}, pure GO and GO-Er excited under 800 nm femtosecond laser, with 70% linear transmittance of all the samples in water/ethanol (1/1, v/v) solution. Obviously, except for $NaYF_4$:Yb^{3+}/Er^{3+} nanoparticles, both GO and GO-Er show very good OL behavior. At high input power density, the output powers are clamped at 137 and 48 mW for GO and GO-Er, respectively. The OL threshold, defined as the input power density at which the transmittance falls to 50% of the linear transmittance, are determined to be 380 mW for GO and 134 mW for GO-Er. This means GO-Er has much better OL effect than GO. Generally, several mechanisms are responsible for OL effect, such as NLS, nonlinear absorption (two-photon absorption, free-carrier absorption, consecutive two-quantum absorption by impurities/dopants, and reverse saturable absorption) and nonlinear refraction.[1,21,22] NLS is reported to be the most common phenomenon for OL in nanoparticles.[23–26] To confirm the contribution of NLS in our samples, we have collected a fraction of scattered light at a forward planar angle of 15^0 and shown in Figure 2b. We can see that the scattered light intensity increased superlinearly with the increasing input optical intensity and the onset of the decrease of transmittance is synchronous with the growth of the scattered light, which proves that NLS plays an important role in the OL.

The NLS centers are comprised of two origins. One is the formation and expansion of solvent bubbles that are induced by the thermal energy transferred from the nanocomposite to the surrounding solvent and will greatly scatter the incident beam and attenuate the incident radiation.[22] It has been proved that this process is more effective under nanosecond pulse laser excitation.[1] Thermal heating induced by a single laser pulse can persist over some characteristic time t_c. As a result, when the time interval between consecutive laser pulses is shorter than t_c, the contribution of thermal effect increases. The time scale of this cumulative process is given by $t_c = \omega^2/4D$, where ω is the beam waist and D is the thermal diffusion coefficient of the materials. Generally, the value of D ranges from 1×10^{-7} to 6×10^{-7} m^2 s^{-1} for organic materials.[26] The calculated t_c is within 1 ms, which is much larger than the time interval between consecutive laser pulses of 12 ns used in our experiment. Therefore, the repetition rate is high enough to cause thermal accumulation effects and

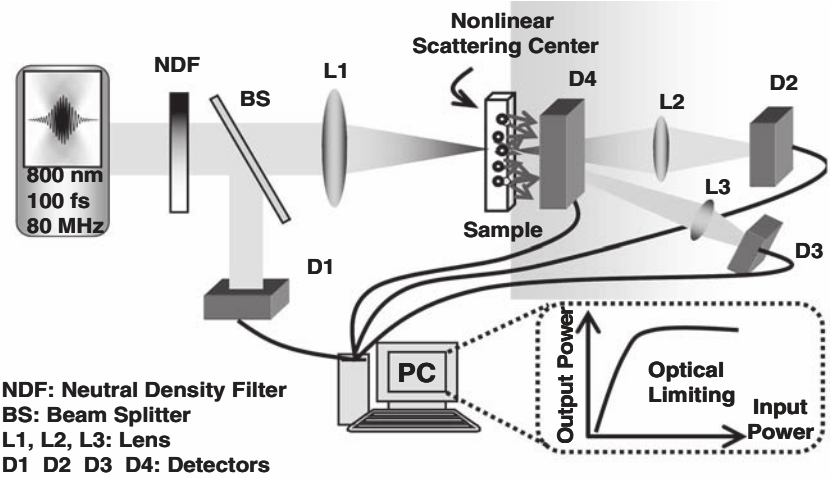

Scheme 1. Optical configurations for the home-built experimental setup used for OL, NLS, and nonlinear absorption measurements.

small NANO MICRO

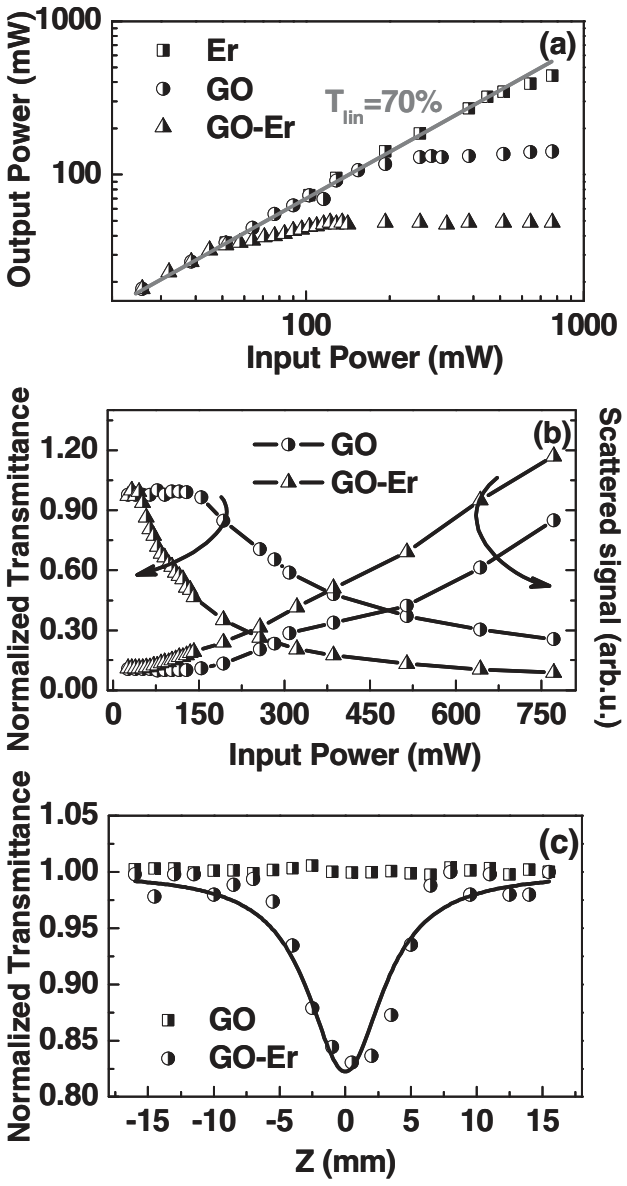

Figure 2. a) OL response of GO, $NaYF_4$:Yb^{3+}/Er^{3+} and GO-Er solutions. b) Normalized nonlinear transmission and scattered signals of GO and GO-Er solutions. c) Open aperture Z-scan data for the measurements of two-photon absorption coefficients in GO and GO-Er.

results in the first type of scattering centers. The second type of scattering centers is generated by the formation and expansion of nanoparticles vapor bubbles due to the sublimation of nanocomposite.[22] This kind of scattering centers can be formed under ultrashort laser pulse excitation with higher power density than that used for the first type of scattering centers. Thus the first and second types of scattering centers should coexist in GO-Er solution.

Figure 2c shows the open aperture Z-scan curves, from which we can obtain the two-photon absorption coefficients. During measurement, the input laser beam was first passed through a beam chopper with an open ratio of 1/10 and a rotating speed of 315 rounds per second. The two-photon absorption coefficient of GO can be negligible compared to GO-Er, which shows strong two-photon absorption behavior. The solid line in Figure 2c is the theoretical fit according to equation:

$$T(z, s=1) = \sum [-q_0(z,0)]^m / (m+1)^{3/2}, \ (q_0(z,0) \le 1) \qquad (1)$$

where $q_0(z,0) = \beta I_0 L_{eff} / (1 + z^2/z_0^2)$, $L_{eff} = [1 - \exp(-\alpha L)]/\alpha$, $z_0 = k\omega_0^2/2$, β is the two-photon absorption coefficient, I_0 is the intensity of the laser beam at focal point z = 0, $L_{eff} = [1 - \exp(-\alpha L)]/\alpha$ is the effective thickness of the sample, α is the linear absorption Acoefficient, and L is the thickness of the sample.[20] In our experiment, the input power density is 5.1 GW cm^{-2}. From the theoretical fit, the two-photon absorption coefficient was determined to be 0.6 cm GW^{-1}. The large two-photon absorption should arise from the increase of π conjugation in GO-Er due to efficient ET process, which coexists with NLS effect to enhance the OL response.

In many cases of open-aperture *Z*-scan measurements, if the detector area is not large enough compared to the size (or transverse distribution region) of the transmitted laser beam, the aperture effect may still be generated even without the actual aperture being placed in front of the detector, which could be remarkably changed due to self-focusing/defocusing and/or thermal lensing effect.[22] The thermal-induced nonlinearity arises from the temporal variation of optical parameters (in particular, refractive index). The laser thermal effect leads to the generation of an acoustic wave that changes the medium density followed by a variation of refractive index. Based on previous reports,[27–29] this process is slow and can be observed in the case of CW radiation, long laser pulses, or in the case of high pulse repetition rate when heat accumulation starts to play an important role. Considering the high repetition rate of the laser we used (80 MHz), thermal lensing can also happen in our experiment, which works as a negative lens, causing the incident beam to defocus and resulting in significant energy blockage by the system aperture (finite detector size). The schematic diagram of the thermal lensing limiter is shown in in **Figure 3**a. The Z-scan measurements can be used to confirm the existence of thermal lensing effect. In order to avoid the electronic nonlinearity, the frequency of beam chopper was set to be 10 Hz, the optical intensity was set to be as low as 0.1 GW cm^{-2}, and the linear transmittance of the aperture was set to be 0.65. The experimental data for GO and GO-Er (closed aperture Z-scan data divided by open aperture) are shown in Figure 3b and the solid curve is the theoretical fit.[20] The normalized transmittance curves with a peak followed by a valley in GO solution indicate that the sign of the nonlinear refraction is negative, i.e., self-defocusing. Therefore, thermal lensing also contributes to OL behavior for GO. However, the thermal lensing in GO-Er is negligible, which may be due to the fast heat dissipation of GO-Er originated from the covalent interaction between the two components. Therefore, it can be concluded that OL for GO results from NSL and thermal lensing effect, which can also be further confirmed by the observation of large refractive-index-change induced nonlinear ring pattern on the transmitted wave front, while the mechanism of enhanced OL in GO-Er, should be due to stronger NLS and two-photon absorption.

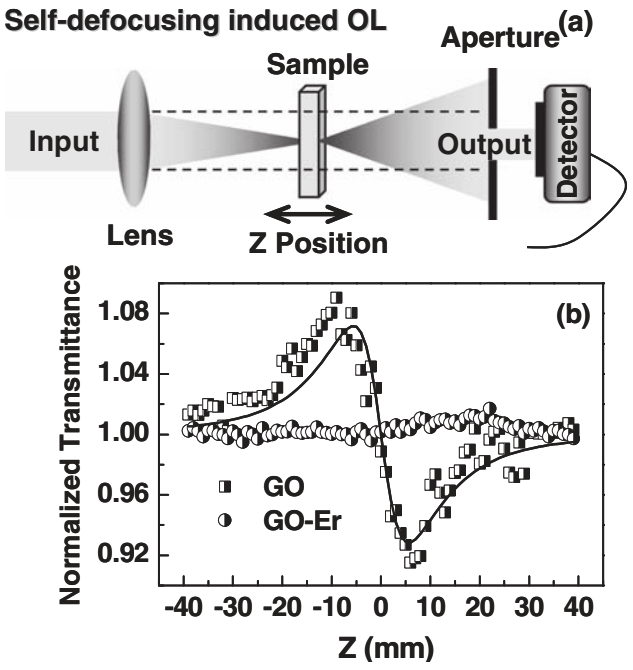

Figure 3. a) Schematic diagram of the thermal lensing limiter. b) Closed aperture Z-scan curves for GO and GO-Er in water/ethanol (1/1, v/v) solutions.

To confirm whether the direct ET from Er^{3+} to GO is feasible or not at 800 nm, we have investigated the OL performance of GO and the nanocomposite of GO/$NaYF_4$:Er^{3+}, where Yb^{3+} ions were not added. As can be seen in **Figure 4**, the final output power is about 120 mW for the nanocomposite and the corresponding OL threshold is 302 mW. Compared to

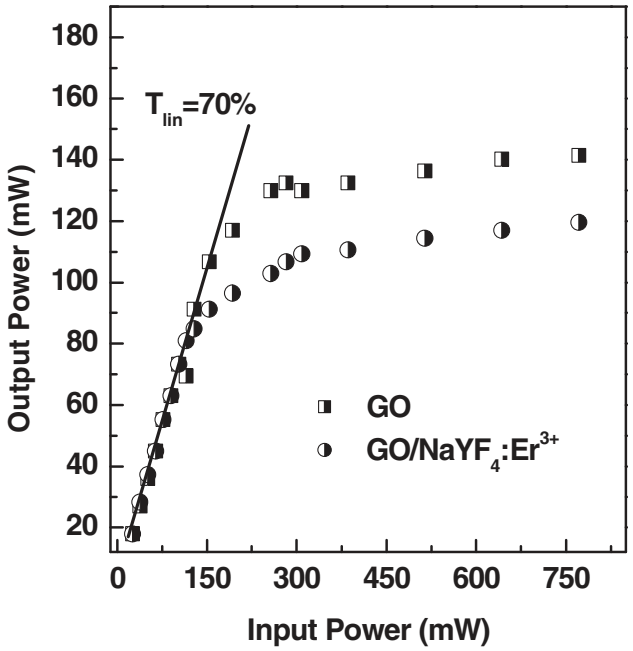

Figure 4. OL response of GO and GO/$NaYF_4$:Er^{3+} solutions, measured with 100 fs and 80 MHz laser pulses at 800 nm. There are no Yb^{3+} ions in GO/$NaYF_4$:Er^{3+}.

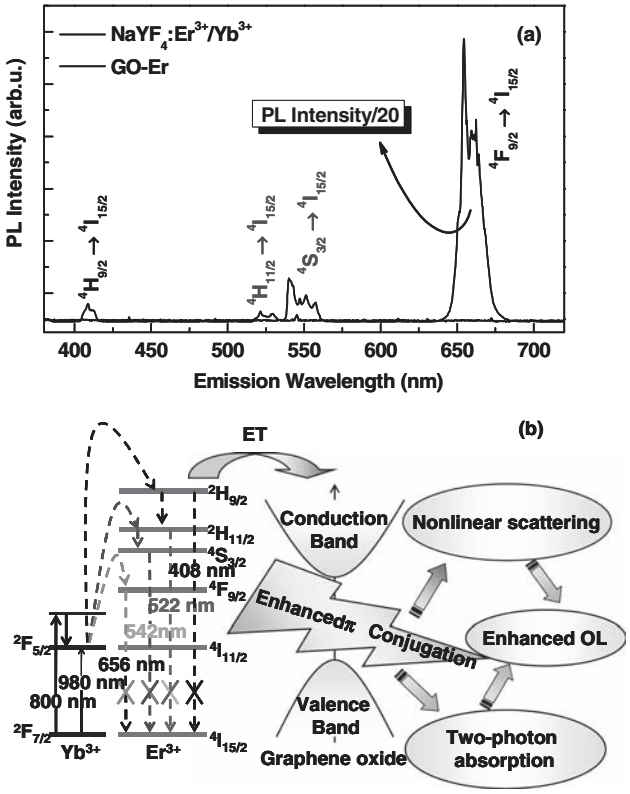

Figure 5. a) Photoluminescence spectra of GO, $NaYF_4$:Yb^{3+}/Er^{3+} nanoparticles, and GO-Er excited by 980 nm CW diode laser. b) Schematic illustration of PL quenching and ET process in GO-Er nanocomposite, leading to the enhanced OL reponse.

GO, there is only slight improvement in OL performance in GO/$NaYF_4$:Er^{3+} nanocomposite, indicating the critical contribution of Yb^{3+} ions in the nanocomposite. With the absence of Yb^{3+}, the ET process can still occur, but at much lower efficiency than that with the presence of Yb^{3+} ions (Figure 2a). This is reasonable because upon excitation, the electrons of Yb^{3+} ions in GO-Er are excited to the energy levels higher than $^2F_{5/2}$, and then relax to $^2F_{5/2}$ (**Figure 5**b). Subsequently, Yb^{3+} ions transfer the energy to the ladder-like energy levels of Er^{3+} ions via multiphoton process at high efficiency. As a result, the efficiency of ET from $NaYF_4$:Yb^{3+}/Er^{3+} to GO is higher than that of GO/$NaYF_4$:Er^{3+}. This process also results in the enhancement of π conjugation of nanocomposite, so the large two-photon absorption is obtained.

As is known, Yb^{3+} ion is a very good photosensitizer and has resonant absorption at 980 nm,[16,30,31] so the ET efficiency from $NaYF_4$:Yb^{3+}/Er^{3+} to GO should be also very high at 980 nm. Figure 5a shows PL spectra of $NaYF_4$:Yb^{3+}/Er^{3+} nanoparticles (synthesized without GO) and GO-Er obtained under 980 nm CW diode laser excitation. $NaYF_4$:Yb^{3+}/Er^{3+} nanoparticles show strong upconversion PL emissions at 408, 522, 542, and 656 nm, which can be ascribed to $^2H_{9/2}$–$^4I_{15/2}$, $^2H_{11/2}$–$^4I_{15/2}$, $^4S_{3/2}$–$^4I_{15/2}$, and $^4F_{9/2}$–$^4I_{15/2}$ transitions, respectively. However, these emission peaks are almost fully quenched in the GO-Er solution, which is obviously due to the appearance of GO. This indicates that there is very efficient energy transfer between GO and $NaYF_4$:Yb^{3+}/Er^{3+}

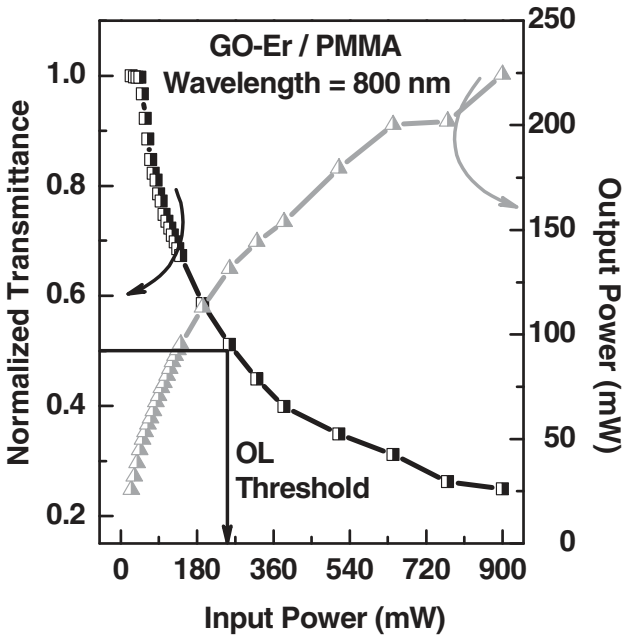

Figure 6. OL response and normalized nonlinear transmittance characteristics of GO-Er in PMMA thin film.

nanoparticles. Figure 5b illustrates the excitation and ET processes from $NaYF_4$:Yb^{3+}/Er^{3+} to GO, which is also the origin of the enhanced OL performance in the nanocomposite. There are two pathways for the PL quenching, i.e., photoinduced electron transfer (PET) and ET. Here GO acts as electron acceptors and $NaYF_4$:Yb^{3+}/Er^{3+} acts as electron donor in their photoexcited state, so PET and/or ET between $NaYF_4$:Yb^{3+}/Er^{3+} and GO could occur.[32–36] As is well know, energy transfer is a distance-dependent interaction between the electronic excited states of GO and $NaYF_4$:Yb^{3+}/Er^{3+} in which excitation is transferred from $NaYF_4$:Yb^{3+}/Er^{3+} to GO through nonradiative dipole–dipole coupling. For effective occurrence of energy transfer, donor and acceptor must be in close proximity (typically small than 10 nm). The covalent bond length (or the spacing) formed between GO and $NaYF_4$:Yb^{3+}/Er^{3+} is roughly estimated to be about 2.5 Å, and the short distance defined by the covalent bond enables high efficient energy transfer between $NaYF_4$:Yb^{3+}/Er^{3+} and GO.

To prove that the large two-photon absorption still contributes to the OL effect in solid state of the GO-Er nanocomposite, we made a thin film sample by mixing GO-Er with poly(methyl methacrylate) (PMMA) at a ratio of 2.5 wt%. In **Figure 6**, we can see that the sample exhibits high linear transmittance (75%) at low-input power density, displaying an OL activity with a threshold of 253 mW while the output power is clamped at 224 mW at high input power density. Since the pure PMMA thin film only gives negligible OL behavior (data not shown), we can claim that the film of GO-Er retains strong two-photon absorption induced OL response under femtosecond laser pulse excitation and the slight decrease of OL is due to the weaker NLS compared to GO-Er solution.

In summary, we have investigated the OL mechanisms of the GO-Er nanocomposite under 800 nm laser pulses (100 fs and 80 MHz). The combination of the enhanced NLS and two-photon absorption, as well as the PET and/or ET between $NaYF_4$:Yb^{3+}/Er^{3+} and GO are responsible for the superior OL behavior. Due to the large two-photon absorption, superior OL behavior in GO-Er is also expected in thin-film samples under the excitation of nanosecond and low-repetition-rate femtosecond pulses. This synergistic effect of the OL mechanisms has provided deep insight for designing new generation OL materials that can work at extended laser wavelengths and pulse domain.

Experimental Section

Materials Synthesis: The nanocomposites have the chemical composition of $NaYF_4$:Yb^{3+}/Er^{3+}, which are typical lanthanide-doped nanoparticles with unique energy upconversion capability and are expected to be used for OL devices in the near-infrared region. The sizes of $NaYF_4$:Yb^{3+}/Er^{3+} nanoparticles vary between 17 to 35 nm with cubic phase. The GO-Er nanocomposites are prepared via a typical solvothermal synthesis method. GO (100 mg) was mixed with $Y(NO_3)_3{\cdot}6H_2O$ (147 mg), $Yb(NO_3)_3{\cdot}5H_2O$ (45 mg), $Er(NO_3)_3{\cdot}5H_2O$ (6.6 mg) and NaF (84.0 mg) in absolute ethanol (40 mL). The mixture was sonicated for 30 min and stirred for another 30 min. The solution was then transferred to a Teflon-lined stainless steel autoclave (50 mL) and heated at 170 °C for 8 h. After cooling down to room temperature, the product was isolated by centrifugation, and was subsequently washed with distilled water and ethanol for several times, and dried at 60 °C. Since GO is rich of carboxylic and hydroxyl groups, it can coordinate with rare earth ions to form a complex, whose principle has been well studied previously.[37]

OL Measurement: The measurements were performed under the excitation of 800 nm laser pulses (100 fs and 80 MHz). The solutions were contained in 1 cm thick quartz cells and were adjusted to have a linear transmittance of 70% at the measured wavelength. The laser beam is split into two parts: reference beam (detector 1), and the excitation beam, which is focused into the center of the solution using a 10 cm focal length lens. The beam size at the focus is calculated to be about 16 μm in radius. The transmitted beam from the solution is slightly focused onto detector 2 by a lens. In this case, the scattering light and defocusing beam induced by thermal-lensing effect at large angle with respect to z axial can not be detected. For the measurement of NLS, a third lens is place at 30° with respect to z axial to collect the scattered light (read out by detector 3). To measure the nonlinear absorption, a fourth detector and a focusing lens with detecting areas much larger than the transmitted beam size was used and placed near the sample (detector 4).

Acknowledgements

Support from the Singapore Ministry of Education through the Academic Research Fund (Tier 1) under Project No. RG63/10 and from the Singapore National Research Foundation through the

Competitive Research Programme (CRP) under Project No. NRF-CRP5-2009-04 is gratefully acknowledged. LH thanks the financial support from the Start-Up Grant (SUG) in NTU and Tier One Grant (RG20/09) from MOE, Singapore.

[1] L. W. Tutt, T. F. Boggess, *Prog. Quant. Electronics* **1993**, *17*, 299.
[2] L. W. Tutt, A. Kost, *Nature* **1992**, *356*, 225.
[3] L. Vivien, P. Lançon, D. Riehl, F. Hache, E. Anglaret, *Carbon* **2002**, *40*, 1789.
[4] N. Izard, P. Billaud, D. Riehl, *Opt. Lett.* **2005**, *30*, 1509.
[5] J. Wang, W. J. Blau, *J. Phys. Chem. C* **2008**, *112*, 2298.
[6] K. S. Novoselov1, A. K. Geim, S. V. Morozov, D. Jiang, Y. Zhang, S. V. Dubonos, I. V. Grigorieva, A. A. Firsov, *Science* **2004**, *306*, 666.
[7] J. Wang, Y. Hernandez, M. Lotya, J. N. Coleman, W. J. Blau, *Adv. Mater.* **2009**, *21*, 2430.
[8] Y. Xu, Z. Liu, X. Zhang, Y. Wang, J. Tian, Y. Huang, Y. Ma, X. Zhang, Y. A. Chen, *Adv. Mater.* **2009**, *21*, 1275.
[9] J. Balapanuru, J. Yang, S. Xiao, Q. Bao, M. Jahan, L. Polavarapu, J. Wei, Q. Xu, K. Loh, *Angew. Chem. Int. Ed.* **2010**, *49*, 6549.
[10] Y. Liu, J. Zhou, X. Zhang, Z. Liu, X. Wan, J. Tian, T. Wang, Y. Chen, *Carbon* **2009**, *47*, 3113.
[11] Z. Liu, Y. Xu, X. Zhang, X. Zhang, Y. Chen, J. Tian, *J. Phys. Chem. B* **2009**, *113*, 9681.
[12] J. Zhu, Y. Li, Y. Chen, J. Wang, B. Zhang, J. Zhang, W. J. Blau, *Carbon*, **2011**, *49*, 1900.
[13] M. Feng, R. Sun, H. Zhan, Yu Chen, *Nanotechnology* **2010**, *21*, 075601.
[14] S. Kumar, M. Anija, N. Kamaraju, K. S. Vasu, K. S. Subrahmanyam, A. K. Sood, C. N. R. Rao, *Appl. Phys. Lett.* **2009**, *95*, 191911.
[15] X. Zhao, Z. Liu, W. Yan, Y. Wu, X. Zhang, Y. Chen, J. Tian, *Appl. Phys. Lett.* **2011**, *98*, 121905.
[16] F. Auzel, *Chem. Rev.* **2004**, *104*, 139.
[17] S. Saxena, T. A. Tyson, S. Shukla, E. Negusse, H. Chen, J. Bai, *Appl. Phys. Lett.* **2011**, *99*, 013104.
[18] X. Huang, Z. Yin, S. Wu, X. Qi, Q. He, Q. Zhang, Q. Yan, F. Boey, H. Zhang, *Small* **2011**, *7*, 1876.
[19] X. Y. Qi, K.-Y. Pu, H. Li, X. Z. Zhou, S. X. Wu, Q.-L. Fan, B. Liu, F. Boey, W. Huang, H. Zhang, *Angew. Chem. Int. Ed.* **2010**, *49*, 9426.
[20] M. Sheik-Bahae, A. A. Said, T. H. Wei, D. J. Haga, E. W. Van Stryland, *IEEE J. Quantum Electron* **1990**, *26*, 760.
[21] G. Gurzadyan, R. K. Ispiryan, *Appl. Phys. Lett.* **1991**, *59*, 630.
[22] G. S. He, L. S. Tan, Q. Zheng, P. N. Prasad, *Chem. Rev.* **2008**, *108*, 1245.
[23] J. Wang, W. J. Blau, *J. Opt. A: Pure Appl. Opt.* **2009**, *11*, 024001.
[24] B. Ananda, S. A. Ntimb, V. Muthukumara, S. S. S. Saia, R. Philipc, S. Mitra, *Carbon*, **2011**, *49*, 4767.
[25] N. Mackiewicz, T. Bark, B. Cao, J. A. Delaire, D. Riehl, W. L. Ling, S. Foillard, E. Doris, *Carbon* **2011**, *49*, 2998.
[26] J. E. Riggs, D. B. Walker, D. L. Carroll, Y. Sun, *J. Phys. Chem. B* **2000**, *104*, 7071.
[27] A. Gnoli, L. Razzari, M. Righini, *Opt. Express* **2005**, *13*, 7976.
[28] A. Nag, A. K. De, D. Goswami, *J. Phys. B: At. Mol. Opt. Phys.* **2009**, *42*, 065103.
[29] M. Falconieri, G. Salvetti, *Appl. Phys. B* **1999**, *69*, 133.
[30] F. Auzel, *C. R. Acad. Sci.* **1966**, *262*, 1016.
[31] F. Auzel, *C. R. Acad. Sci.* **1966**, *263*, 819.
[32] N. S. Sariciftci, L. Smilowitz, A. J. Heeger, F. Wudl, *Science* **1992**, *258*, 1474.
[33] X. Qi, K. Pu, X. Zhou, H. Li, B. Liu, F. Boey, W. Huang, H. Zhang, *Small* **2010**, *6*, 663.
[34] L. Q. Xu, L. Wang, B. Zhang, C. H. Lim, Y. Chen, K. Neoh, E. Kang, G. Fu, *Polymer* **2011**, *52*, 2376.
[35] D. Lee, T. Kim, M. Lee, *Chem. Commun.* **2011**, *47*, 8259.
[36] A. Ghosh, K. V. Rao, S. J. George, C. N. R. Rao, *Chem. Eur. J.* **2010**, *16*, 2700.
[37] Z. Bian, C. Huang, in *Electroluminescence Based on Lanthanide Complexes, in Rare Earth Coordination Chemistry: Fundamentals and Applications* (ed: C. Huang), John Wiley & Sons, Ltd, Chichester, UK **2010**, Ch.11.

Received: February 2, 2012
Published online: May 21, 2012

